Constant and High Switching Frequency Torque Controller for DTC Drives

C. L. Toh, N. R. N. Idris, *Senior Member, IEEE*, and A. H. M. Yatim, *Senior Member, IEEE*

***Abstract*—The letter presents a new method of increasing the switching frequency of a direct torque control (DTC) of induction machines. The method simply replaces the hysteresis comparator of the conventional DTC drives with a triangular waveform-based constant switching frequency controller. By synchronizing the digital signal processor (DSP) sampling with a triangular waveform and with an appropriate systematic controller design, a high switching frequency DTC drive is possible without requiring a high-frequency space-vector modulator. The implementation of the controller is simple and operates based on waveform comparisons; in this letter it is implemented using a combination of a DSP and a field programmable gate array device. Simulation and experimental results indicate that the controller both reduces the torque ripple and maintains a constant switching frequency.**

***Index Terms*—Ac drives, direct torque control, induction motor drives.**

I. Introduction

DIRECT torque control (DTC) of induction motors has gained popularity in industrial applications mainly due to its simple control structure. Since it was first introduced in 1986 [1], several modifications and improvements have been made to the original control structure in order to overcome two main problems normally associated with the conventional DTC drive; namely the high electromagnetic torque ripple and variable switching frequency. It is well established that these problems are mainly due to the hysteresis torque controller. Since the magnitude of the torque ripple for an inverter-fed electrical machine is inversely proportional to the inverter switching frequency, appreciable torque ripple reduction can be achieved by increasing the inverter switching frequency. Most of the DTC drive torque ripple reduction methods in the literature are centered around this concept.

In hysteresis-based DTC, torque ripple can be reduced by reducing the width of the hysteresis band. This, however, can lead to an extremely high switching frequency. If digital hysteresis-based DTC is chosen, torque overshoot or undershoot beyond the hysteresis band is inevitable due to the discrete sampling. As with other hysteresis-based systems, a hysteresis-based DTC drive results in a variable switching frequency that depends on operating conditions, in particular the speed. Perhaps the most practical solution for increasing the switching frequency (thus reducing the torque ripple) while at the same time maintaining a constant switching frequency, as chosen by most researchers, is to use the space vector modulation-based DTC (SVM-DTC) [2]. In order to obtain a small torque ripple in a SVM-DTC drive with digital implementation, a fast processor is required.

This letter presents a new high-switching-frequency torque controller for the DTC of an IM drive. The controller does not require a space vector modulator, and it is capable of producing constant switching frequency regardless of drive operating conditions. Furthermore, the implementation of the controller is simple and the drive control structure is similar to the conventional hysteresis-based DTC drive. A similar controller was introduced in [3] and [4]; however, the one presented in this letter switches at a much higher frequency. The higher switching frequency is made possible by implementing the controller using the combination of a digital signal processor (DSP) and FPGA. In this letter, the principle and method of the controller design are discussed. Some simulation and experimental results are also presented to show the effectiveness of the controller in increasing the switching frequency, as well as in maintaining a constant switching frequency.

II. Structure and Modeling of the Proposed Torque Controller

The DTC drive with the proposed controller and the structure of the controller is shown in Fig. 1. The proposed torque controller consists of two triangular waveform generators, two comparators and a proportional integral (PI) controller. The two triangular waveforms ($\mathrm{C_{upper}}$ and $\mathrm{C_{lower}}$) are 180° out of phase with each other. The absolute values of the dc offsets for the triangular waveforms are set to half of their peak-peak values. As indicated in Fig. 1(b), the output of the controller, which can be $1, 0$ or -1, is similar to the hysteresis controller. This means that similar voltage vectors look-up tables, as in the conventional DTC drive, can be used. The value of the instantaneous output of the torque controller designated by $q_t(t)$ is given by (1). For a triangular period of $\mathrm{T_{tri}}$, its averaged value which will be designated by $\mathrm{d_t(t)}$ is given by (2)

$$\mathrm{q_t(t)} = \begin{cases} 1, & \text{for } \mathrm{T_c} \geq \mathrm{C_{upper}} \\ 0, & \text{for } \mathrm{C_{lower}} < \mathrm{T_c} < \mathrm{C_{upper}} \\ -1, & \text{for } \mathrm{T_c} \leq \mathrm{C_{lower}} \end{cases} \tag{1}$$

$$\mathrm{d_t(t)} = \frac{1}{\mathrm{T_{tri}}} \int_{\mathrm{t}}^{\mathrm{t+T_{tri}}} \mathrm{q(t)dt}. \tag{2}$$

In order to design the controller systematically, it is necessary to obtain the linear model of the torque loop. In general, the procedure is similar to the method for obtaining a linear model of

Manuscript received January 16, 2005; revised May 19, 2005. Recommended by Associate Editor P. L. Chapman.

The authors are with the Department of Energy Conversion, Fakulti Kejuruteraan Elektrik, Universiti Teknologi Malaysia, 81310 UTM, Johor, Malaysia (e-mail: nikrumzi@ieee.org).

Digital Object Identifier 10.1109/LPEL.2005.851316

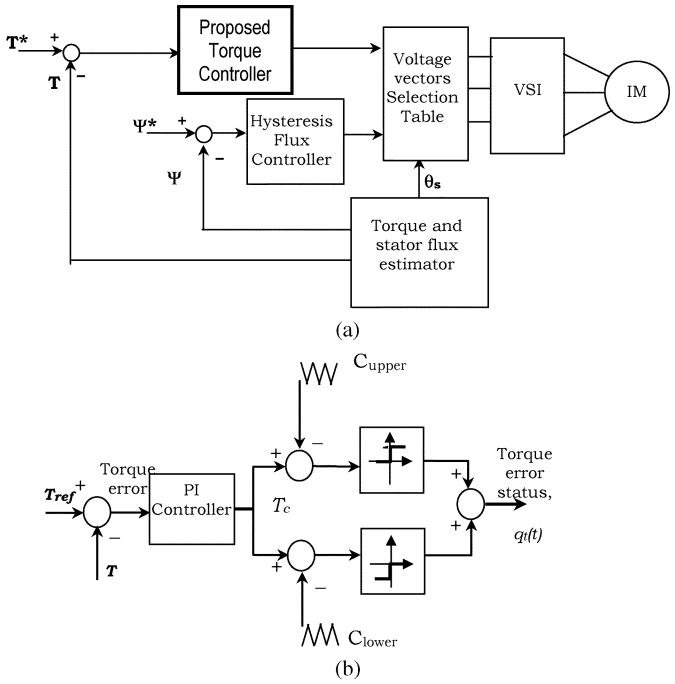

Fig. 1. Proposed high-switching-frequency torque controller. (a) DTC structure with the proposed controller. (b) Functional block diagram of the controller.

any power electronic systems. The full procedure for modeling the torque loop is given in [4] and is briefly discussed here. In the general reference frame, the equations used to model the induction machine are given as follows:

$$\overline{\mathrm{v}}_{\mathrm{s}}^{\mathrm{g}} = \mathrm{R}_{\mathrm{s}}\overline{\mathrm{i}}_{\mathrm{s}}^{\mathrm{g}} + \frac{\mathrm{d}\overline{\psi}_{\mathrm{s}}^{\mathrm{g}}}{\mathrm{dt}} + \mathrm{j}\omega_{\mathrm{g}}\overline{\psi}_{\mathrm{s}}^{\mathrm{g}} \tag{3}$$

$$0 = \mathrm{R}_{\mathrm{r}}\overline{\mathrm{i}}_{\mathrm{r}}^{\mathrm{g}} + \frac{\mathrm{d}\overline{\psi}_{\mathrm{r}}^{\mathrm{g}}}{\mathrm{dt}} + \mathrm{j}(\omega_{\mathrm{g}} - \omega_{\mathrm{r}})\overline{\psi}_{\mathrm{r}}^{\mathrm{g}} \tag{4}$$

$$\overline{\psi}_{\mathrm{s}}^{\mathrm{g}} = \mathrm{L}_{\mathrm{s}}\overline{\mathrm{i}}_{\mathrm{s}}^{\mathrm{g}} + \mathrm{L}_{\mathrm{m}}\overline{\mathrm{i}}_{\mathrm{r}}^{\mathrm{g}} \tag{5}$$

$$\overline{\psi}_{\mathrm{r}}^{\mathrm{g}} = \mathrm{L}_{\mathrm{r}}\overline{\mathrm{i}}_{\mathrm{r}}^{\mathrm{g}} + \mathrm{L}_{\mathrm{m}}\overline{\mathrm{i}}_{\mathrm{s}}^{\mathrm{g}}. \tag{6}$$

In the above equations, $\overline{\psi}_{\mathrm{s}}^{\mathrm{g}}$ and $\overline{\psi}_{\mathrm{r}}^{\mathrm{g}}$ are the stator and rotor flux linkages, respectively. $\overline{\mathrm{v}}_{\mathrm{s}}^{\mathrm{g}}$, $\overline{\mathrm{i}}_{\mathrm{s}}^{\mathrm{g}}$, and $\overline{\mathrm{i}}_{\mathrm{r}}^{\mathrm{g}}$ are the stator voltage, stator current, and rotor current space vectors, respectively. L_{s}, L_{r} and L_{m} are the stator self inductance, rotor self inductance and mutual self inductance, respectively. The super-script "g" in the above equations denotes that the quantities are referred to the rotating general reference frame. ω_{g} and ω_{r} are the speeds of the general reference frame and rotor, respectively. The torque and mechanical dynamics of the machine are modeled by the following:

$$\mathrm{J}\frac{\mathrm{d}\omega_{\mathrm{m}}}{\mathrm{dt}} = \mathrm{J}\frac{2}{\mathrm{p}}\frac{\mathrm{d}\omega_{\mathrm{r}}}{\mathrm{dt}} = \mathrm{T}_{\mathrm{e}} - \mathrm{T}_{\mathrm{load}} \tag{7}$$

$$\mathrm{T}_{\mathrm{e}} = \frac{3}{2}\frac{\mathrm{p}}{2}\overline{\psi}_{\mathrm{s}}^{\mathrm{g}} \times \overline{\mathrm{i}}_{\mathrm{s}}^{\mathrm{g}}. \tag{8}$$

J and p are the moment of inertia and number of poles, respectively, and ω_{m} is the mechanical rotor speed.

Using (1)–(6), in the stationary reference frame, it can be shown [5] that the positive and negative torque slopes are given by

$$\frac{\mathrm{dT}_{\mathrm{e}}^{+}}{\mathrm{dt}} = -\mathrm{T}_{\mathrm{e}}\left(\frac{1}{\sigma\tau_{\mathrm{s}}} + \frac{1}{\sigma\tau_{\mathrm{r}}}\right) + \frac{3}{2}\frac{\mathrm{p}}{2}\frac{\mathrm{L}_{\mathrm{m}}}{\sigma\mathrm{L}_{\mathrm{s}}\mathrm{L}_{\mathrm{r}}}\left(\overline{\mathrm{v}}_{\mathrm{s}} - \mathrm{j}\omega_{\mathrm{r}}\overline{\psi}_{\mathrm{s}}\right) \bullet \mathrm{j}\psi_{\mathrm{r}} \tag{9}$$

$$\frac{\mathrm{dT}_{\mathrm{e}}^{-}}{\mathrm{dt}} = -\mathrm{T}_{\mathrm{e}}\left(\frac{1}{\sigma\tau_{\mathrm{s}}} + \frac{1}{\sigma\tau_{\mathrm{r}}}\right) - \frac{3}{2}\frac{\mathrm{p}}{2}\frac{\mathrm{L}_{\mathrm{m}}}{\sigma\mathrm{L}_{\mathrm{s}}\mathrm{L}_{\mathrm{r}}}\mathrm{j}\omega_{\mathrm{r}}\overline{\psi}_{\mathrm{s}} \bullet \mathrm{j}\psi_{\mathrm{r}} \tag{10}$$

where σ is the total flux linkage factor, and τ_{r} and τ_{s} are the rotor and stator time constants, respectively. Equation (10) assumes that zero voltage vectors are selected to reduce the torque. Since the instantaneous stator flux frequency can be obtained in terms of the average synchronous frequency and the duty ratio [4], (7) and (8) can be written in the stator flux reference frame as given in (11) and (12)

$$\frac{\mathrm{dT}_{\mathrm{e}}^{+}}{\mathrm{dt}} = -\mathrm{A}_{\mathrm{t}}\mathrm{T}_{\mathrm{e}} + \mathrm{B}_{\mathrm{t}}\mathrm{v}_{\mathrm{s}}^{\psi\mathrm{s}} + \mathrm{K}_{\mathrm{t}}\left(\frac{\omega_{\mathrm{e}}}{\mathrm{d}} - \omega_{\mathrm{r}}\right) \tag{11}$$

$$\frac{\mathrm{dT}_{\mathrm{e}}^{-}}{\mathrm{dt}} = -\mathrm{A}_{\mathrm{t}}\mathrm{T}_{\mathrm{e}} - \mathrm{K}_{\mathrm{t}}\omega_{\mathrm{r}} \tag{12}$$

where $\mathrm{A}_{\mathrm{t}} = 1/\sigma\tau_{\mathrm{sr}}$ $\mathrm{B}_{\mathrm{t}} = (3\mathrm{p}/4)(\mathrm{L}_{\mathrm{m}}/\sigma\mathrm{L}_{\mathrm{s}}\mathrm{L}_{\mathrm{r}})\psi_{\mathrm{s}}$ $\mathrm{K}_{\mathrm{t}} = (3\mathrm{p}/4)(\mathrm{L}_{\mathrm{m}}/\sigma\mathrm{L}_{\mathrm{s}}\mathrm{L}_{\mathrm{r}})(\psi_{\mathrm{s}}\psi_{\mathrm{r}}^{\psi_{\mathrm{s}}})$ and $1/\sigma\tau_{\mathrm{sr}} = (1/\sigma\tau_{\mathrm{s}}) + (1/\sigma\tau_{\mathrm{r}})$

In the above equations, it is assumed that the stator and rotor fluxes are constant and the q components of the selected voltage vectors are zero. In other words, the voltage vectors are tangential to the circular stator flux locus. Finally, the average torque equation over one triangular frequency can be written as (13). Transforming (13) to the frequency domain, the torque loop, as shown in Fig. 2, can be constructed

$$\frac{\mathrm{dT}_{\mathrm{e}}}{\mathrm{dt}} = -\mathrm{A}_{\mathrm{t}}\mathrm{T}_{\mathrm{e}} + \mathrm{B}_{\mathrm{t}}\mathrm{v}_{\mathrm{s}}^{\psi\mathrm{s}}\mathrm{d} + \mathrm{K}_{\mathrm{t}}(\omega_{\mathrm{slip}}). \tag{13}$$

III. Design of the Proposed Torque Controller

With the linearized torque loop, the torque control bandwidth can be set using suitable PI controller parameters. The bandwidth is chosen such that it satisfies the maximum bandwidth limited by the DSP sampling frequency or the triangular frequency, depending on which is lower. This means that the triangular frequency can be set to a frequency higher than the sampling frequency, as long as it is synchronized with the sampling of the DSP, and the torque bandwidth is much lower than the sampling frequency. The triangular frequency was set to 10 kHz and the sampling of the DSP was synchronized with the peak of the triangular waveform, i.e., sampling frequency of 20 kHz. The bandwidth is limited to a maximum of 1 kHz, which is constrained by the triangular frequency. It should be noted that it is also possible to increase the triangular frequency, e.g., to 40 kHz, with the sampling retained at 20 kHz. In this case, the bandwidth is limited to 2 kHz, which is an order lower than the DSP sampling frequency. Obviously, as the switching frequency is increased, the switching losses will also increase. However, since the switching frequency of the proposed controllers is fixed and known, the switching losses are predictable. This is not true for the hysteresis-based controllers, due to the variable switching frequency.

TABLE I
CONTROL AND MOTOR PARAMETERS

Stator resistance, R_s	10.9 Ω
Rotor resistance, R_r	9.5 Ω
Stator self-inductance, L_s	0.859 H
Rotor self-inductance, L_r	0.859 H
Mutual inductance, L_m	0.829 H
Combined inertia, J	0.00286 kg-m^2
No. of poles, p	2

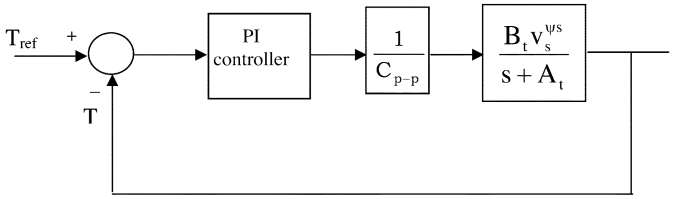

Fig. 2. Linearized torque loop.

Using the induction machine parameters in Table I and the torque loop in Fig. 2, the Bode plot of the uncompensated open-loop gain of the torque loop is shown in Fig. 3. The zero of the PI controller was set such that it canceled the pole of the system at 355. With the zero fixed at this value, the gain was adjusted to the desired bandwidth. From simulation and experimental results, it was found that the torque loop bandwidth of about 300 Hz gives excellent torque response with very little overshoot and zero steady-state error. The corresponding PI controller's parameters for this setting were $\mathrm{K_p} = 180$, $\mathrm{K_i} = 60\,000$. The Bode plots of the open-loop gain with the controller are shown in Fig. 3.

IV. SIMULATION AND EXPERIMENTAL RESULTS

The large-signal simulations of the DTC induction motor drive with the proposed and hysteresis-based controllers were performed using MATLAB-SIMULINK. The parameters of the PI controller, obtained as described in the previous section, were used in the simulation. To show the feasibility of the proposed controller, an experiment was also carried out for both the hysteresis and proposed controllers. The set-up of the experiment as shown in Fig. 4, consists of a dSPACE controller card based on a TMS320C31 DSP, an IGBT-based voltage source inverter (VSI), a standard 1/4 HP squirrel cage induction machine coupled to a dc machine, and an ALTERA FPGA. The DSP was used to estimate the torque and stator flux at a sampling frequency of 20 kHz and to implement the PI controller of the proposed torque controller. The FPGA was used to implement the hysteresis and proposed controllers, including the generation of the 10-kHz triangular waveform of the proposed controller, to perform the comparison, and to implement the voltage vector table and selections, as well as to generate the blanking time for the VSI. The parameters of the induction motor as tabulated in Table I were used in the simulation as well as in the experiment. The hysteresis band of the hysteresis-based controller was set to 10% of the rated

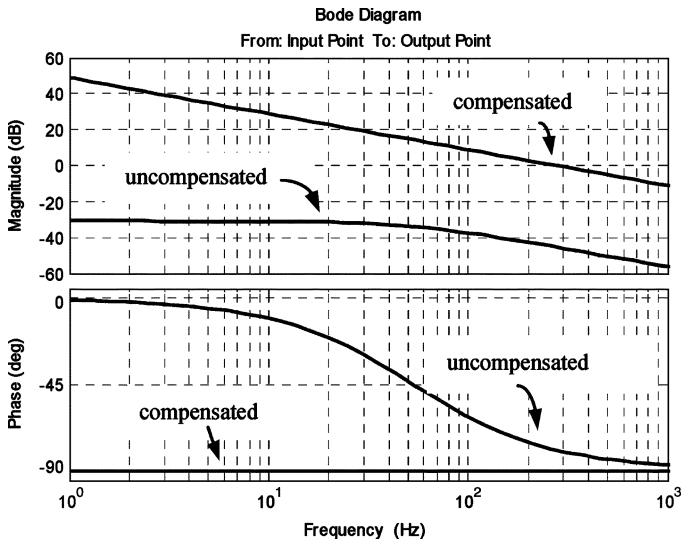

Fig. 3. Bode diagram of the uncompensated and compensated torque loop.

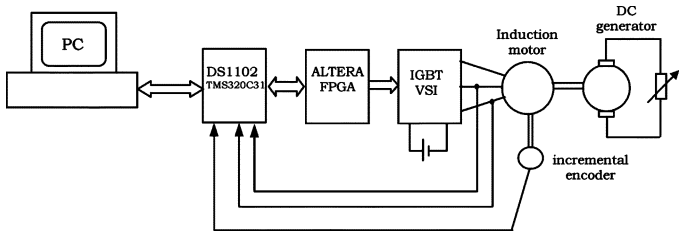

Fig. 4. Experimental setup.

torque value. The simulation results of step torque responses for the hysteresis and proposed torque controllers are shown in Fig. 5(a). The corresponding experimental results are given in Fig. 5(b). The hysteresis-based simulation results show smaller peak-peak ripple compared to the experimental results because no torque delay was included in the simulation. In actual implementation, even a small delay results in a significant increase in torque ripple [4]. Fig. 5 clearly indicates that the dynamics of the proposed controller are comparable to the hysteresis-based controller, in spite of the significant torque reduction.

Fig. 6(a) shows the waveforms obtained from the simulation and experiment of the upper and lower triangular waveforms which were compared with the output of the PI controller. The comparison was performed within the FPGA and the waveforms were recorded at steady-state speed. The bottom trace is the result of the comparison which was then fed to the voltage-vector selection table. For the experimental results, the low signal indicates a zero vector was selected, whereas a high signal indicates that an active vector was selected. For the proposed controller, no reverse voltage was selected. The simulation and experimental results obtained for the hysteresis-based controller are shown in Fig. 6(b). The hysteresis comparison of the torque error is also performed within the FPGA. The torque error status of -1 in the simulation indicates that the reverse voltage vector (instead of zero voltage) is selected. For the experimental waveform, the results of the comparison consist of two bits: the first bit is high when reverse voltage is selected and the second bit is high when the forward voltage vector is selected.

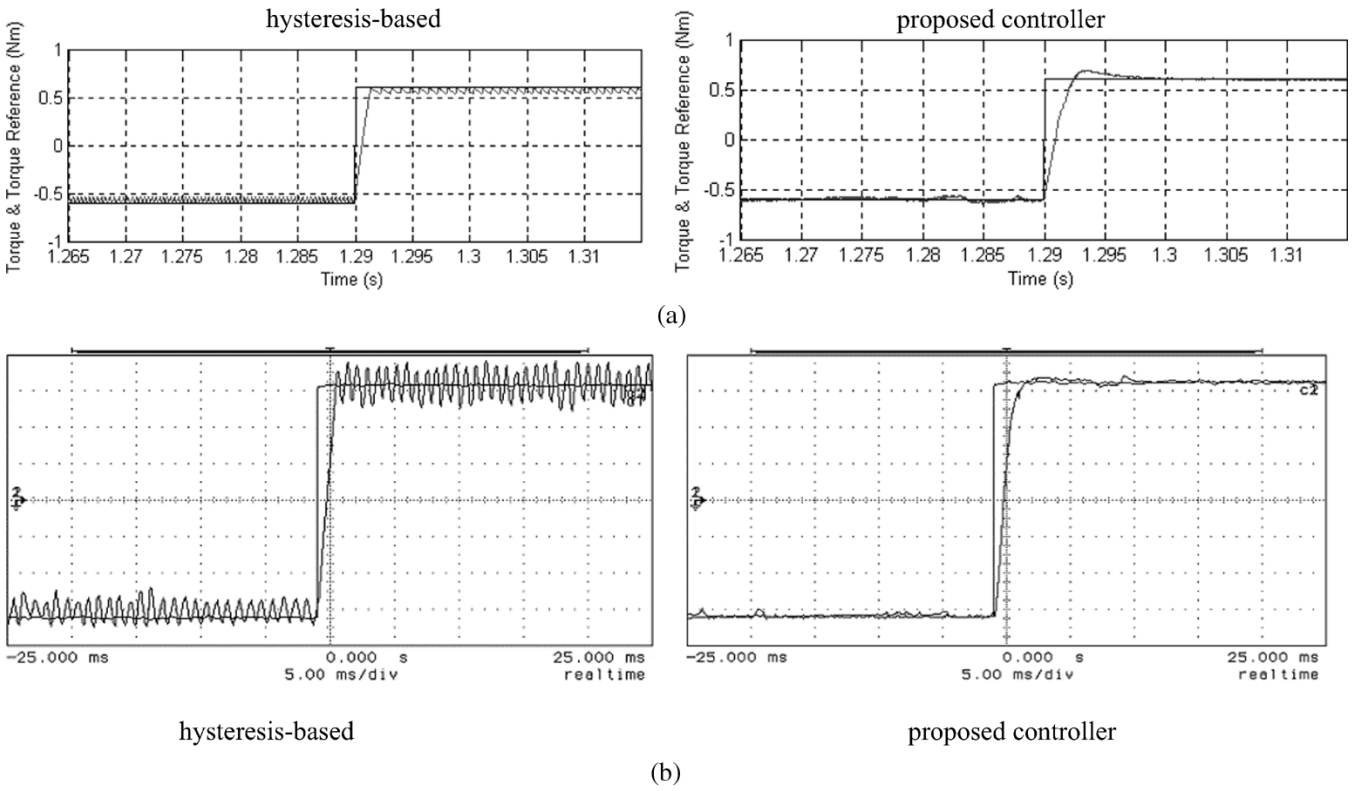

Fig. 5. Responses for a step torque of 1.2 Nm. (a) Simulation: hysteresis and proposed controller. (b) Experiment: hysteresis and proposed torque (0.2 Nm/div).

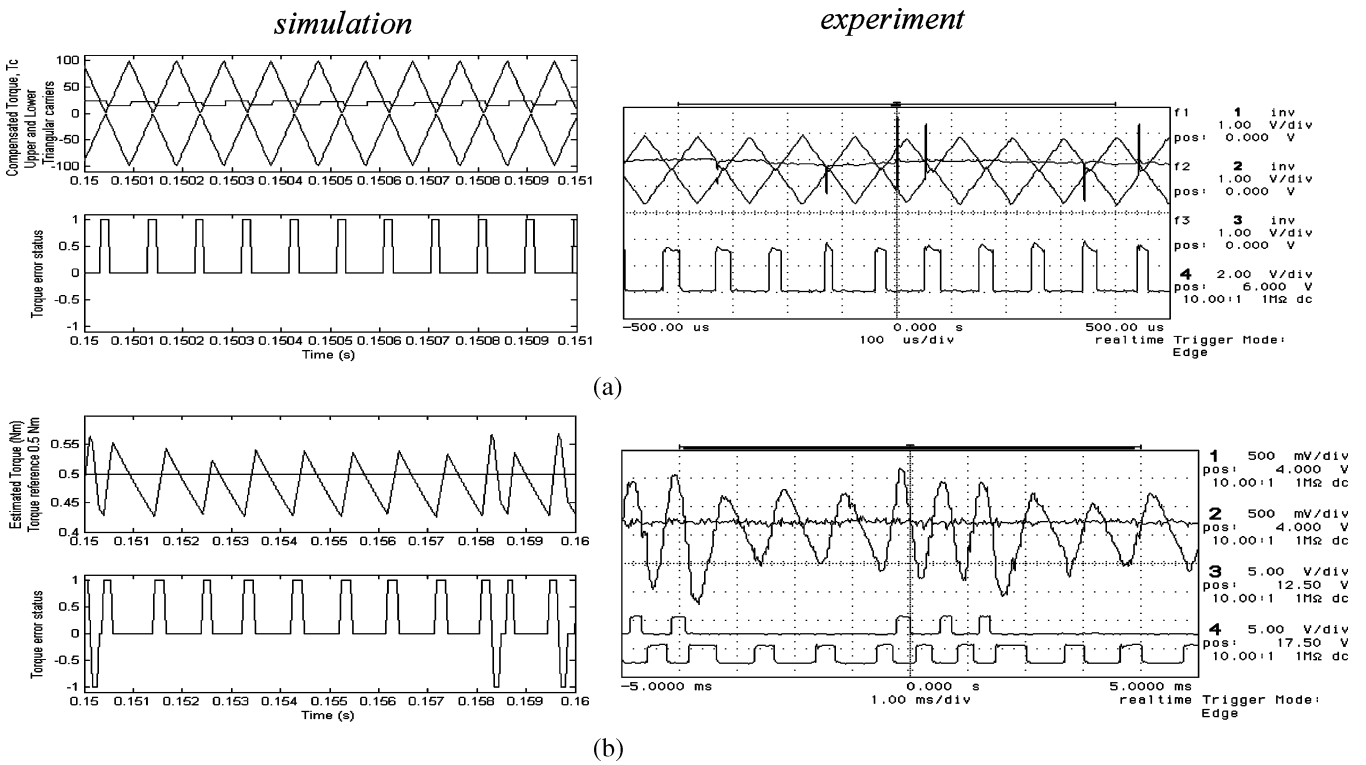

Fig. 6. Simulation and experimental waveforms. (a) Proposed controller. (b) Hysteresis-based controller.

Owing to the delay in torque feedback, reverse vectors are selected that consequently increase the torque ripple [3].

Fig. 7(a) gives the experimental results of the speed and torque response obtained using the proposed controller when a square wave torque reference of ± 0.6 Nm at 1 Hz was applied. Next, a speed loop was constructed with the speed feedback obtained using a low-resolution incremental encoder (200 ppr). The speed and torque response for a square-wave

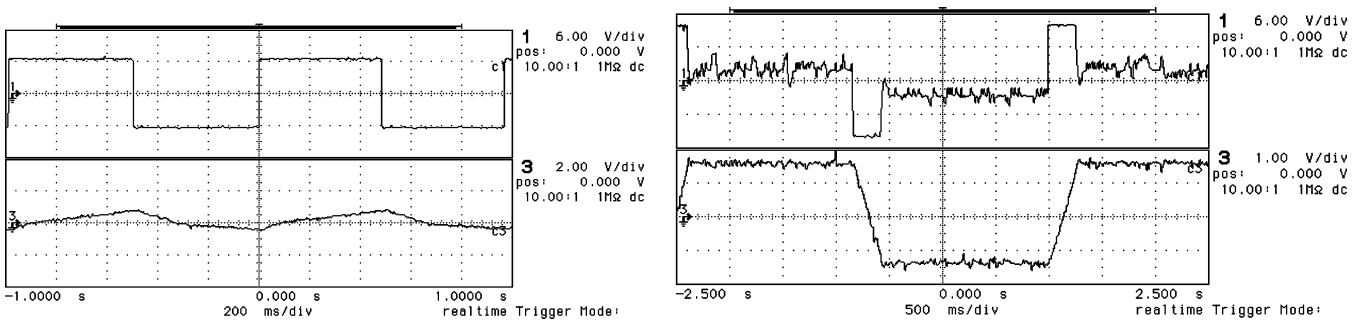

(a) (b)

Fig. 7. Experimental results for the proposed controller (upper—torque, lower—speed). (a) Square-wave torque reference for torque: 0.6 Nm/div; speed: 18.67 $\mathrm{rads}^{-1}/\mathrm{div}$. (b) Square-wave speed reference for torque: 1 Nm/div; speed: 9.33 $\mathrm{rads}^{-1}/\mathrm{div}$.

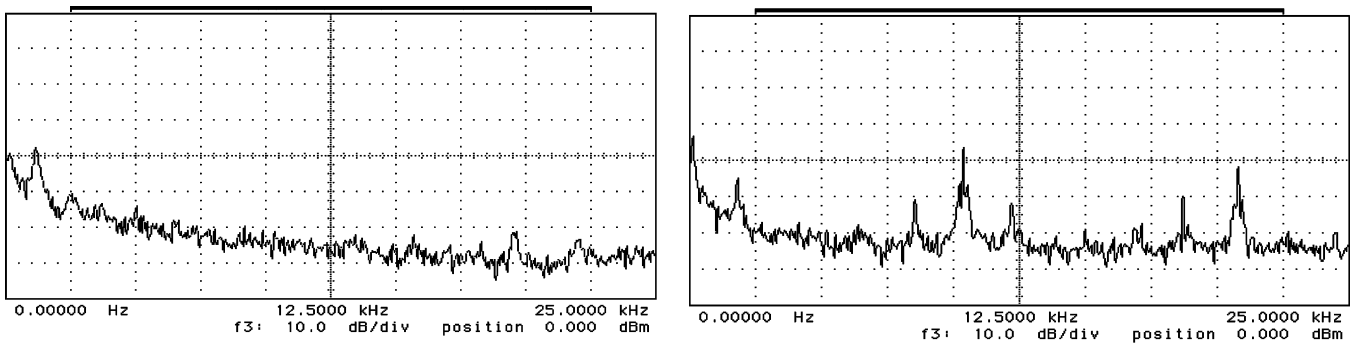

(a) (b)

Fig. 8. Frequency spectrum of the phase voltage. (a) Hysteresis-based controller. (b) Proposed controller.

speed reference of ± 24 rad/s at about 3 Hz is shown in Fig. 7(b). The results in Fig. 9 indicate that the proposed controller gives an excellent dynamic response with the DTC drive.

Finally, the drives of both the hysteresis and proposed controller, respectively, were run with a square-wave torque reference. The corresponding frequency spectrums of the phase voltage for both drives are shown in Fig. 8. For the proposed torque controller, the dominant harmonic is at the triangular frequency of about 10 kHz. On the other hand, a spread spectrum with an unpredictable switching frequency is obtained for the hysteresis-based controller.

V. Conclusion

This letter has presented an alternative method of increasing the switching frequency for a DTC induction motor drive system. The proposed method not only increased the frequency, but also to retained the frequency at a fixed value regardless of the rotor speed. The simple structure of the originally proposed DTC drive by Takahashi is retained by replacing the hysteresis comparator with the fixed frequency controller. The implementation of the controller is shown to be very simple, as it involves only waveform comparisons and thus can be performed using a digital circuit or an FPGA. The experimental results showed that with the increased frequency, the torque ripple is significantly reduced.

References

[1] I. Takahashi and T. Noguchi, "A new quick-response and high-efficiency control strategy of an induction motor," *IEEE Trans. Ind. Appl.*, vol. IA-22, no. 5, pp. 820–827, Oct. 1986.

[2] G. S. Buja and M. P. Kazmierkowski, "Direct torque control of PWM inverter-fed ac motors—a survey," *IEEE Trans. Ind. Electron.*, vol. 51, no. 4, pp. 744–757, Aug. 2004.

[3] N. R. N. Idris and A. H. M. Yatim, "Reduced torque ripple and constant torque switching frequency strategy for direct torque control of induction machine," in *Rec. IEEE Applied Power Electronics Conf.*, 2000, pp. 154–161.

[4] ——, "Direct torque control of induction machines with constant switching frequency and reduced torque ripple," *IEEE Trans. Ind. Electron.*, vol. 51, no. 4, pp. 758–767, Aug. 2004.

[5] D. Casadei and G. Serra, "Analytical investigation of torque and flux ripple in DTC schemes for induction motors," in *Rec. IEEE Industrial Electronics Conf.*, 1997, pp. 552–556.